Bioorganic Chemistry 86 (2019) 482–493

Contents lists available at ScienceDirect

Bioorganic Chemistry

journal homepage: www.elsevier.com/locate/bioorg

Synthesis, crystal structure and biological evaluation of new phosphoramide derivatives as urease inhibitors using docking, QSAR and kinetic studies

Khodayar Gholivand[a,*], Mahsa Pooyan[a], Fahimeh Mohammadpanah[a], Foroogh Pirastefar[a], Peter C. Junk[b], Jun Wang[b], Ali Asghar Ebrahimi Valmoozi[a], Ahmad Mani-Varnosfaderani[a]

[a] Department of Chemistry, Faculty of Science, Tarbiat Modares University, Tehran, Iran
[b] College of Science & Engineering, James Cook University, Townsville, Queensland 4811, Australia

ARTICLE INFO

Keywords:
Bisphosphoramide derivatives
Urease enzyme
Inhibitory activity
Docking
Kinetics
QSAR

ABSTRACT

In an attempt to achieve a new class of phosphoramide inhibitors with high potency and resistance to the hydrolysis process against urease enzyme, we synthesized a series of bisphosphoramide derivatives (**01–43**) and characterized them by various spectroscopic techniques. The crystal structures of compounds **22** and **26** were investigated using X-ray crystallography. The inhibitory activities of the compounds were evaluated against the jack bean urease and were compared to monophosphoramide derivatives and other known standard inhibitors. The compounds containing aromatic amines and their substituted derivatives exhibited very high inhibitory activity in the range of IC_{50} = 3.4–1.91 × 10^{-10} nM compared with monophosphoramides, thiourea, and acetohydroxamic acid. It was also found that derivatives with P═O functional groups have higher anti-urease activity than those with P═S functional groups. Kinetics and docking studies were carried out to explore the binding mechanism that showed these compounds follow a mixed-type mechanism and, due to their extended structures, can cover the entire binding pocket of the enzyme, reducing the formation of the enzyme-substrate complex. The quantitative structure-activity relationship (QSAR) analysis also revealed that the interaction between the enzyme and inhibitor is significantly influenced by aromatic rings and P═O functional groups. Collectively, the data obtained from experimental and theoretical studies indicated that these compounds can be developed as appropriate candidates for urease inhibitors in this field.

1. Introduction

Control and inhibition of urease enzyme is the most important step in agricultural productivity and the treatment of diseases caused by enzyme disorders. The urease enzyme is present in a variety of microorganisms, such as some eukaryotes and prokaryotes, and as a catalyst converts urea into ammonia and carbon dioxide or carbamate during the reaction of hydrolysis [1–3]. The high and uncontrolled activity of urease results in excessive ammonia release and increased pH of the environment, bringing about damaging consequences in medicine and agriculture, such as gastrointestinal infections and destruction of plant roots [2,4–12]. Inhibition of urease enzyme seems to be the only way to deal with these negative consequences. Among various compounds identified as urease inhibitors, monophosphoramide derivatives are broadly considered as the most effective ones [1,13–16]. Despite their high inhibitory ability, these compounds have attracted less attention due to their instability in aqueous media [17]. In order to overcome this issue, the compounds containing a P−C linkage (phosphonates and phosphinates) have been reported to be good substitutes for the monophosphoramide compounds, which have exhibited relatively less inhibitory activity than the monophosphoramides [9,18,19]. Regarding the mentioned problem, in this work, we introduced a new framework for phosphoramides with high hydrolytic stability as urease inhibitors. Several studies have demonstrated that the functional groups of P═O and P−N in monophosphoramide derivatives have the largest effect on enzyme inhibition [5,9,15,19–21]. Inspired by these reports, we considered the various categories of bisphosphoramide derivatives containing functional groups of P═O and P−N as urease inhibitors. Accordingly, 43 bisphosphoramides were offered with the general formula of $(R_1)(R_2)P(Y)X(Y)P(R_1)(R_2)$ (Y = O and S; R_1 and R_2 = C_6H_5, C_6H_5O, C_6H_5NH, C_2H_5O; X = various aliphatic and aromatic diamines). Out of the compounds, 26 of them were reported in our previous publications [22–27] and others were newly synthesized in the present study, see Fig. 1.

In continuation of the work, the inhibitory activity of these compounds was evaluated against the jack bean urease and compared to the

* Corresponding author.
E-mail address: gholi_kh@modares.ac.ir (K. Gholivand).

https://doi.org/10.1016/j.bioorg.2019.01.064
Received 1 November 2018; Received in revised form 20 January 2019; Accepted 27 January 2019
Available online 08 February 2019

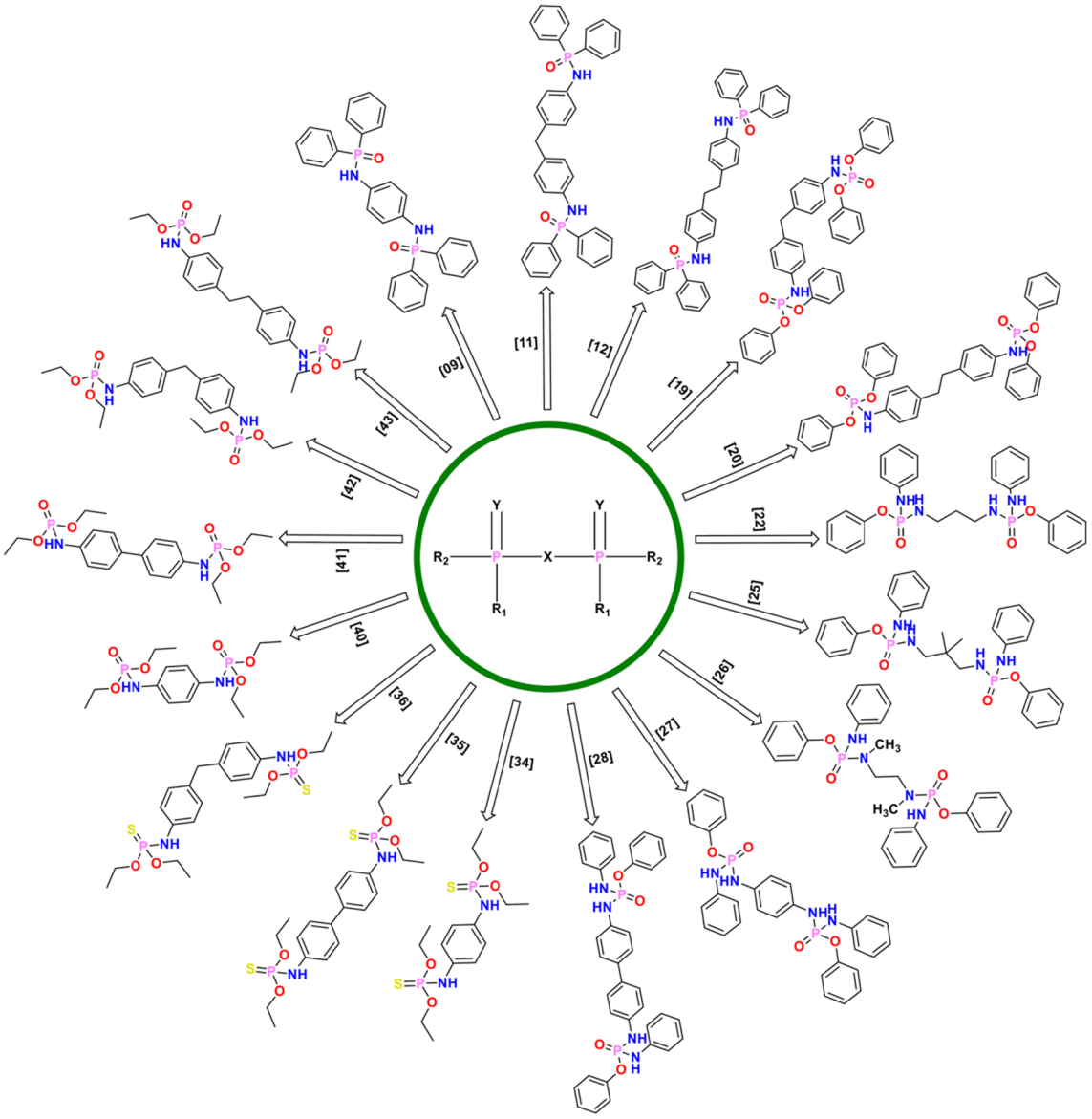

Fig. 1. Schematic of newly synthesized compounds in the present work.

previously reported monophosphoramides [1,2,5,6,15,20,21,28]. Kinetic and docking studies were conducted to explore the mode of interaction and also to gain an insight into the reason behind the relatively high difference in inhibitory activity of these compounds with monophosphoramides. Also, structural parameters affecting the inhibitory activity of the compounds were obtained through QSAR studies using Genetic Algorithm-Artificial Neural Networks (GA-ANN).

In general, with the aim of developing and improving the hydrolytic stability of urease inhibitors, a new framework for phosphoramide inhibitors of urease enzyme with high potency and resistance to the hydrolysis process was introduced. Furthermore, by using computational and experimental methods the mechanism of interaction between these compounds with the urease enzyme, as well as significant factors affecting this interaction were explored.

2. Results and discussion

2.1. Chemistry

Bisphosphoramide derivatives (**01–43**) were synthesized from the reaction of 2 mmol of $R_1R_2P(O)Cl$ with 1 mmol of the corresponding diamine in the presence of triethylamine in acetonitrile or dichloromethane solution at 0 °C according to our previously reported procedures [22–27]. The pathway for the synthesis of target compounds is described in Scheme 1. The structures of synthesized derivatives were characterized by FT-IR, ^{1}H NMR, ^{13}C NMR, ^{31}P NMR spectroscopy techniques, and elemental analysis. Also, the structures of compounds **22** and **26** were furthermore identified by X-ray single-crystal structure analysis. Bisphosphoramides **09**, **11**, **12**, **19**, **20**, **22**, **25–28**, **34–36** and **40–43** have been synthesized for the first time and their structure and purity were also confirmed by spectral data. A summary of these data is presented in Table 1. In addition, six monophosphoramide derivatives were synthesized [6,29] to investigate their inhibitory properties and to compare them with bisphosphoramide derivatives under identical conditions (Fig. 3B).

In the IR spectra of the newly synthesized compounds, two bonds appeared in the range of 1185–1295 cm^{-1} and 811–815 cm^{-1}, which are assigned to the P=O and P=S groups, respectively (Table 1). The absorption bands of the P–N stretching vibrations for all compounds were found in the range of 754–982 cm^{-1}. The ^{31}P NMR chemical shift of these compounds was observed to be in two different ranges of −6.4

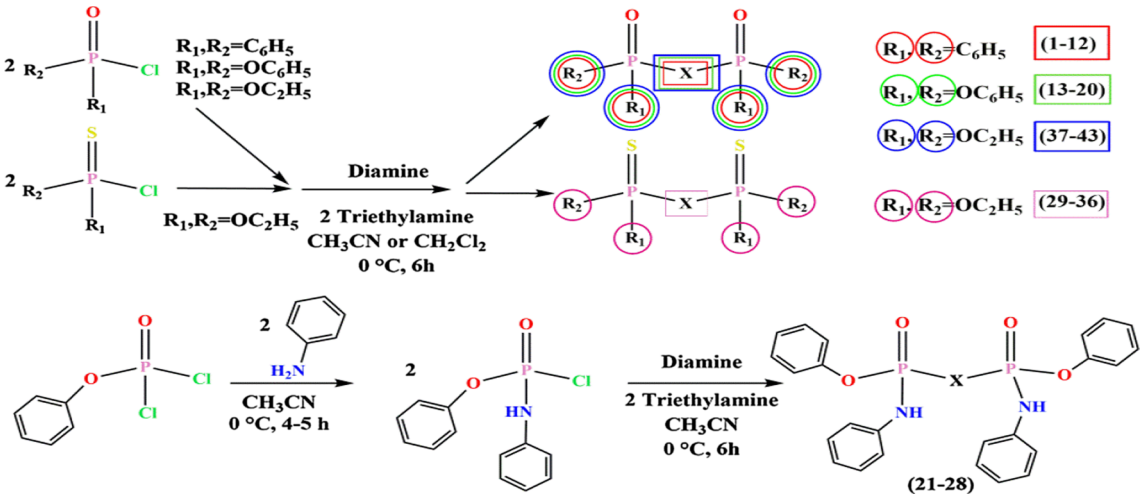

Scheme 1. Synthetic route of bisphosphoramide derivatives, each color represents a category of bisphosphoramide derivatives with their corresponding diamines.

to 16.23 ppm and also 64.35–69.5 ppm, attributed to derivatives containing, respectively, P═O and P═S groups. Comparison of the ^{31}P NMR spectra of the newly synthesized compounds shows that the phosphorus chemical shifts of the compounds **19** and **20**, resulted from the strong inductive effect of the phenoxy groups, shift to lower field and appear in the range of −6.41 to −6.48 ppm. The ^{1}H NMR spectra of the compounds **34–36** and **40–43** display triplet and multiplet signals at around 1.08 and 3.68 ppm, which are related to the methyl and the methylene protons in the CH_3-CH_2 and OCH_2 groups, respectively. In the ^{1}H NMR spectra of compounds **11, 12, 19** and **20**, the methylene protons have appeared as a multiplet signal in the range of 2.99–3.57 ppm. The ^{1}H NMR and ^{31}P NMR results presented here are in good agreement and consistent with the previously reported spectral results for the corresponding compounds [22–24,26]. See Supplementary Information for full details the spectral data.

2.2. Crystal structure analysis of compounds *22* and *26*

For X-ray analysis, suitable single crystals of compounds **22** and **26** were obtained by a slow evaporation method using methanol solvent. X-ray crystallographic data and ORTEP diagrams of both compounds **22** and **26** are shown in Table 2 and Fig. 2A, respectively. Selected bond distances and angles are listed in Table S1 (see the Supporting Information). The X-ray diffraction data analysis reveals that **22**

Table 1
A summary of the spectral data of newly synthesized compounds.

com	FT-IR data (KBr pellet, cm^{-1}): selected bands:	^{1}H NMR (500.13 MHz, d6–DMSO, 25 °C, TMS); δ=	^{31}P NMR (202.45 MHz, d6-DMSO, 25 °C, H_3PO_4 external); δ = ppm
09	1195 s (P═O), 960 s (P–N).	6.76 (s, 4H, C_6H_4), 6.61 (d, 2H, NH), 7.28–8.15 (m 10H C_6H_5).	16.1 (d)
11	1185 s, (P═O), 1119 s, 931 m, 725 m (P–N).	3.32–3.57 (m, 2H, CH_2), 8.09 (d, 2H, $^{2}J_{PH}$ = 12.1 Hz, NH).	16.20 (d)
12	1193 s (P═O), 929 m (P–N).	3.16–3.43 (m, 4H, CH_2), 8.10 (d, 2H, $^{2}J_{PH}$ 11.45 Hz, NH).	16.23 (d)
19	1196 s (P═O), 1000 m, 946 m (P–O), 764 m, (P–N).	2.99–3.01 (m, 2H, CH_2), 8.77 (d, 2H, $^{2}J_{PH}$ = 10.20 Hz, NH).	−6.48 (d)
20	1232 s, 1185 s (P═O), 991 s, 943 s (P–O), 762 m (P–N).	3.12–3.41 (m, 4H, CH_2), 8.69 (d, 2H, $^{2}J_{PH}$ = 10.75 Hz, NH).	−6.41 (d)
22	1208 s (P═O), 941 (P–O), 758 (P–N).	1.44–1.49 (m, 2H, CH_2–CH_2), 2.79–2.85 (m, 4H, CH_2–CH_2), 5.19 (m, 2H, NH).	5.46 (m)
25	1209 s (P═O), 937 (P–O), 756 (P–N).	^{1}H NMR (300.13 MHz): 0.61–0.81 (m, 6H, CH_3), 3.34–3.70 (m, 4H, C-CH_2), 5.26 (m, 2H, NH).	6.04
26	1220 (P═O), 922 (P–O), 756 (P–N).	2.49–2.57 (m, 6H, N–CH_3), 3.07–3.15 (m, 4H, CH_2–N).	6.79 (m)
27	1205 s (P═O), 1072w, 991 m (P–O), 933 s, 754 m (P–N).	^{1}H NMR (300.13 MHz): 5.31 (d, 2H, $^{2}J_{PH}$ = 9.69 Hz, NH).	3.31 (d)
28	1209 s (P═O), 1064 s (P–O), 922 m, 755 m (P–N).	6.37 (m, 2H, NH).	3.6 (d)
34	1028 s (P–O), 956 s (P–N), 811 s (P═S).	1.08 (t, 12H, $4CH_3$), 3.68–4.45 (m, 8H, $4CH_2$).	69.5 (d)
35	1028 (P–O), 965 m (P–N), 815 m (P═S).	^{1}H NMR (300.13 MHz): 1.09–1.44 (t, 12H, CH_3), 3.68–4.42 (m, 8H, OCH2), 8.64 (d, 1H, $^{2}J_{PH}$ = 8.30 Hz, NH).	^{31}P NMR (121.49 MHz): 64.35 (d)
36	1024 s (P–O), 959 s (P–N), 814 m (P═S).	1.17–1.19 (t, 12H, CH_3), 3.71 (s, 2H, CH_2), 3.93–4.03 (m, 8H, OCH2), 8.25 (d, 1H, $^{2}J_{PH}$ = 8.09 Hz, NH).	65.63 (d)
40	1212 s (P═O), 1038 s (P–O), 982 s (P–N).	1.19 (t, 12H, $4CH_3$), 3.95–4.50 (m, 8H, $4CH_2$).	2.9 (d)
41	1224 s (P═O), 1027 s (P–O), 976 m (P–N).	^{1}H NMR (300.13 MHz): 1.19–1.24 (t, 12H, CH_3), 3.92–4.06 (m, 8H, OCH2), 8.03 (d, 1H, $^{2}J_{PH}$ = 9.30 Hz, NH).	^{31}P NMR (121.49 MHz): 2.52 (d)
42	1224 s (P═O), 1027 s (P–O), 976 m (P–N).	^{1}H NMR (300.13 MHz): 1.16–1.21 (t, 12H, CH_3), 3.65 (s, 2H, CH_2), 3.86–3.92 (m, 8H, OCH2), 7.85 (d, 1H, $^{2}J_{PH}$ = 9.26 Hz, NH).	^{31}P NMR (121.49 MHz): 2.72 (d)
43	1235 s (P═O), 1040 s (P–O), 972 m (P–N).	^{1}H NMR (300.13 MHz): 1.16–1.21 (t, 12H, CH_3), 2.48 (m, 4H, CH_2), 4.00–3.92 (m, 8H, OCH2), 7.82 (d, 1H, $^{2}J_{PH}$ = 9.00 Hz, NH).	^{31}P NMR (121.49 MHz): 2.81 (d)

Table 2
Crystal data and structural refinement parameters for compounds **22** and **26.**

Compound	22	26
Empirical formula	$C_{27}H_{30}N_4O_4P_2$	$C_{28}H_{32}N_4O_4P_2$
Formula weight	536.49	550.52
T(K)	100(2)	100(2)
Crystal system, space group	monoclinic, $P2_1/c$	monoclinic, $P2_1/c$
a (Å)	10.735(2)	12.1461(4)
b (Å)	9.851(2)	13.4965(4)
C (Å)	24.672(5)	8.9082(3)
α	90	90
β	92.99(3)	102.250(10)
γ	90	90
V	2605.5(9)	1427.07(8)
Z	4	2
D_{calc} (Mg m^{-3})	1.368	1.281
Absorption coefficient (mm^{-1})	0.208	0.192
F(0 0 0)	1128	580
Crystal size (mm)	0.9 × 0.3 × 0.01	0.25 × 0.20 × 0.20
θ range for data collection (°)	1.9–24.99	1.72–30.57
Limiting indices	$-12 \le h \le 12$ $-11 \le k \le 11$ $-27 \le l \le 28$	$-17 \le h \le 17$ $-19 \le k \le 19$ $-12 \le l \le 12$
Total reflections	19,407	31,888
Unique reflections (R_{int})	4353 [$R_{(int)}$ = 0.0614]	4384[$R_{(int)}$ = 0.0186]
Completeness to θ(%)	94.8% (θ = 25.00)	99.9% (θ = 30.57)
Data/restraints/parameters	4353/0/335	4384/0/173
Refinement method	Full-matrix least squares on F^2	Full-matrix least squares
Goodness-of-fit (GOF) on F^2	1.163	1.002
Final R indices [$I > 2\sigma(I)$]	R_1 = 0.0578, wR_2 = 0.1546	R_1 = 00340, wR_2 = 0.1030
R indices (all data)	R_1 = 0.0644, wR_2 = 0.1579	R_1 = 0.0369, wR_2 = 0.1071
Largest difference in peak and hole (e Å^{-3})	0.458 and −0.503	0.413 and −0.311

crystallizes in the monoclinic space group $P2_1/c$ and its asymmetric unit contains one molecule. In this molecule, two phosphoryl groups are found in the *syn* direction toward each other. Due to the different orientations of the phenoxy and phenylamino rings attached to the phosphorus atoms and the different torsion angles of phosphorus atoms (N3-P2-N4-C16 = 62.0(3)°), (N2-P1-N1-C1 = –55.4(4)°), the molecule doesn't have an inversion center (Table S1). In the crystal structure, each molecule is connected to six neighboring molecules via N3-H3···O1, N2-H2···O1 and N4-H4···O3 (dH3···O1 = 2.005, dH2···O1 = 2.027 and dH4···O3 = 2.030 Å) hydrogen bonds (Table S2), leading to the formation of two-dimensional layers consisting of $R_2^1(8)$, $R_3^3(18)$ and $R_3^2(10)$ rings along the ab-plane, as shown in Fig. 2B. Single-crystal X-ray structural analysis of **26** indicates that it crystallizes in a monoclinic system, space group $P2_1/c$ and contains half of the molecule in the asymmetric unit and the other half is created by a center of inversion.

Compared to **22**, in this molecule, the phosphoryl groups are in the opposite direction from each other, and due to the replacement of hydrogen substitutes attached to nitrogen atoms with methyl groups, each molecule is connected to only four neighboring molecules through four hydrogen bonds (N1-H1N···O1 (dH1N···O1 = 1.958 (8))) (Table S2). These connections lead to the creation of two-dimensional layers consisting of $R_4^4(26)$ rings along the *bc*-plane, (Fig. 2C). Therefore, it can be expected that when the functional groups attached to nitrogen atoms change from methyl to hydrogen, different positions can be provided for binding to active sites of urease enzyme. Further information about the crystal packing is given in the "Support Information".

2.3. Urease inhibitory activity

Five categories of bisphosphoramide compounds, including bis(P,P-diphenyl phosphinicamide), bis(diethyl phosphoramidate), bis(diphenyl phosphoramidate), bis((phenylamino)(phenoxy)phosphinicamide), bis(diethyl phosphoramidothioate) (see Fig. 3A), with different aliphatic and aromatic diamines, were synthesized and their inhibitory activity was determined *in vitro*. The results of the inhibition assays against jack bean urease are presented in Table 3. In this analysis, the inhibitory activity of some monophosphoramides was also evaluated as shown in Fig. 3B. Phenylphosphorodiamidate (PPD) was used as the reference compound for the assay, and its value is also given in Fig. 3B. The results of inhibition analysis indicated that derivatives containing aromatic diamines with long spacers between the two amino groups and aromatic substituted derivatives such as phenyl and phenoxy groups have a higher inhibitory effect than others. These derivatives with a range of IC_{50} = 3.4–1.91 × 10^{-10} nM have greater inhibitory potency than the positive control (with IC_{50} of 21 nM) and other known standard inhibitors such as thiourea and acetohydroxamic acid [30,31]. Compared to the monophosphoramides activities reported in this work

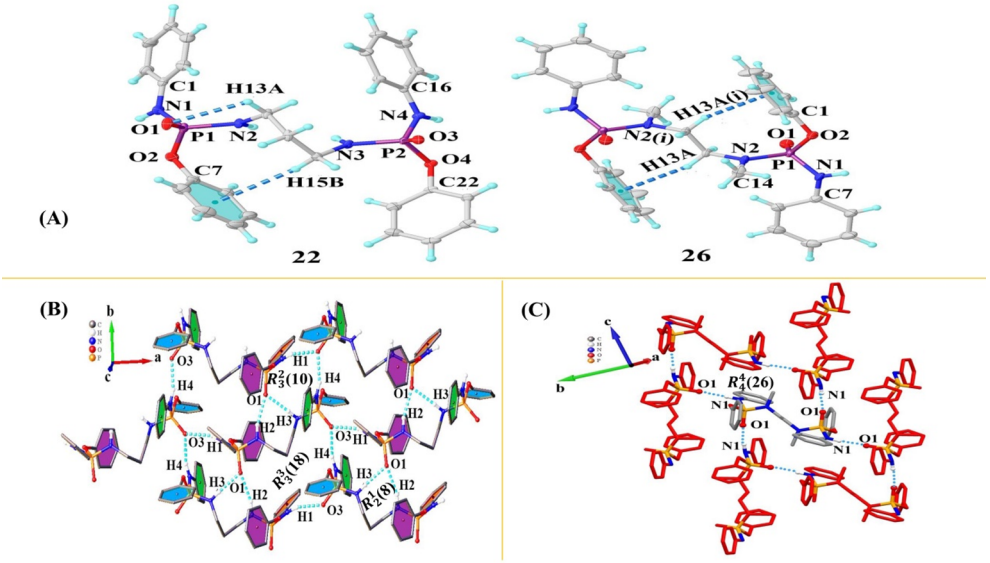

Fig. 2. (A) ORTEP diagrams for the molecular structure of 22 and 26 (the thermal ellipsoids are drawn at the 50% probability level) with the atom-numbering scheme and schematic representation of intramolecular hydrogen bonds. Symmetry code: i: -x, -y, 1-z. (B) 2D representation of hydrogen bond interactions in *ab*-plane, which shows each molecule is connected to six neighboring molecules through hydrogen bond interactions. (C) Representation of the hydrogen bonding interactions in 26.

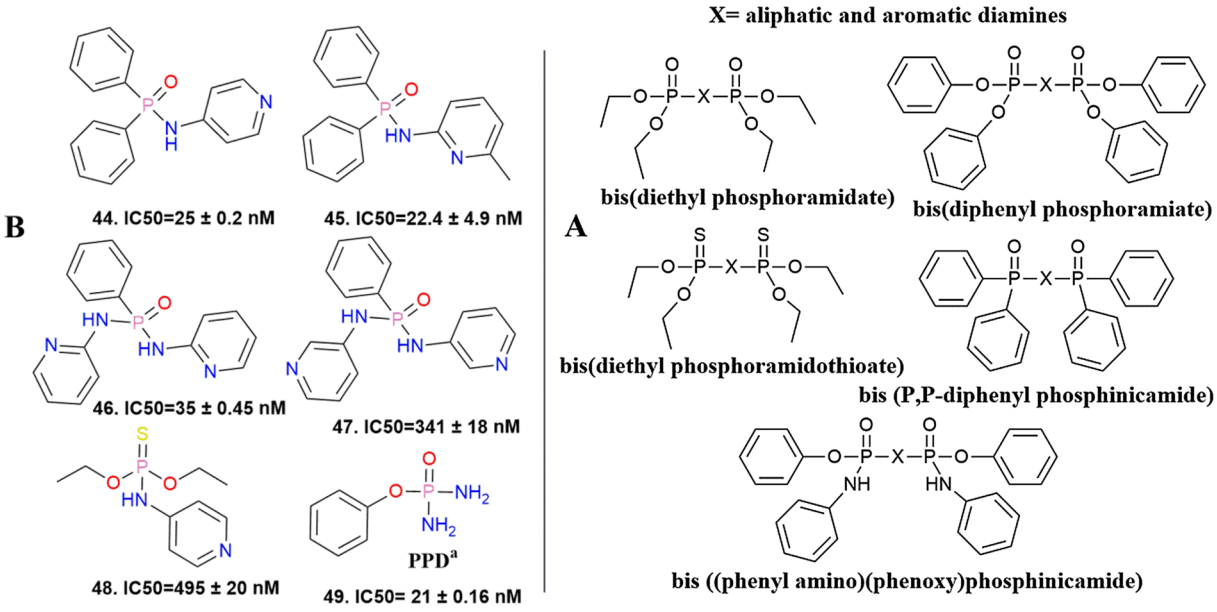

Fig. 3. (A) Five categories of synthesized bisphosphoramide compounds. (B) Inhibitory amounts of monophosphoramide compounds. PPD[a] (PPD was used as reference).

(IC_{50} = 21–495 nM) and previously reported monophosphoramides [1,2,5,6,15,20,21,28], these group of compounds show potent inhibitory activities against jack bean urease. Among the derivatives of bisphosphoramide containing aromatic diamines, Compound **12** with IC_{50} of 1.91 ± 0.03 × 10^{-10} nM is considered as one of the most potent inhibitors. The change in the substitutions attached to the phosphorus atoms from phenyl to ethoxy caused a significant reduction in inhibition activity. On the other hand, the displacement of the P═O moiety with the P═S moiety led to a sharp decrease in inhibition activity. In general, the category of compounds of bis diethyl phosphoramidothioate containing aliphatic diamines (with IC_{50} = 11,200–23,000 μM) showed the least inhibitory activity and the category of bis P,P-diphenyl phosphinicamide compounds with aromatic diamines (with IC_{50} = 1.91 × 10^{-13}–0.0028 μM) showed the highest inhibitory activity in this assay. According to these interpretations, aromatic diamines and the P═O moiety have a significant effect on the inhibitory activity of these derivatives. These results were supported by a molecular docking study, so that the investigation of the binding energy values clearly indicated that the lowest and highest binding energy belongs to compounds **12** (–9.05 kcal/mol) and **30** (–3.45 kcal/mol), respectively, which indicates the high affinity of **12** for interaction with urease enzyme. Data related to the binding energy of the compounds are listed in Table 3.

2.4. Kinetics of urease inhibition by compound 12

G.W. McCarty and co-workers determined the inhibitory mechanism of the monophosphoramide compounds [21]. These derivatives have a slow-binding competitive inhibitory mechanism that competes with urea due to their small structure and similarity to urea substrates for binding to the same location. The inhibitory mechanism of bisphosphoramide derivatives against the urease enzyme has not been investigated so far. We expected these compounds to have a different mechanism due to their extended structure and high inhibitory activity compared to monophosphoramide derivatives. To conduct kinetic studies, **12** was selected as the most active compound for determining the mechanism of urease inhibition. The data obtained from Lineweaver–Burk plots revealed a mixed–type mechanism for **12**, in which, K_m andV_{max}, in the presence of composition **12** increased and decreased respectively (see Fig. 4A). The values of K_i and K_I were calculated by plotting separate graphs of slopes and y-intercepts of the Lineweaver–Burk plot versus the concentration of inhibitor respectively [32], (Fig. 4(B) and (C)). Obtained values of K_i and K_I were 5.7 × 10^{-5} and 0.014 μM respectively, revealing the strong tendency of the compound **12** to the free jack bean urease. It has been argued that this compound, due to its extended structure, can encompass all binding sites of the enzyme, thus reducing the possible formation of the enzyme-substrate complex.

2.5. Structural analysis of docking

To explain and understand the mechanism of enzyme inhibition and binding mode of bisphosphoramide derivatives inside the binding pocket of enzyme, molecular docking of these compounds on the crystal structure of jack bean urease was investigated. According to Fig. 5A, the results obtained from molecular docking showed that π–π stacking, π–sulphur interaction, hydrogen bonds and hydrophobic interactions are the main interactions between bisphosphoramide derivatives and urease enzyme and that these compounds completely covered the binding pocket due to their extended structures. Docking results including the free energy of binding ($\Delta G_{binding}$) and inhibition constant (Ki) are presented in Table 3 and Table S5, respectively. One of the strategies to inhibit enzymes is to restrict flap mobility. The Cys592 residue (also known as CME592) is one of the most important residues of jack bean urease and is located on the mobile flap at the active site entrance. The interaction of the compounds with Cys592 significantly reduces the activity of the enzyme. In the analysis of compounds binding model, it was observed that π–sulphur interactions of phenyl substituents of bisphosphoramides with flap residues Cys592 and hydrogen bonding or π–alkyl interactions of compounds with flap residue Arg439 are constant in compounds containing aromatic rings. The compound **12** with −9.05 kcal/mol binding free energy and inhibition constant 231.92 nM has the best interaction with the enzyme compared to other compounds. As shown in Fig. 5A, the binding mode of **12** is such that it covers the entire catalytic site. There are four interactions involving hydrogen bonding interactions between **12** and the active site residues. The first interaction is between the P═O oxygen atom of compound **12** and the amino group of His593 (d = 1.78 Å), and the second and third interactions are observed separately between each of the two amine groups of Arg609 and the P═O oxygen atom (the length

Table 3
Inhibitory activity (IC_{50}), binding energy and experimental and predicted pIC_{50} values of the synthesized bisphosphoramide derivatives against jack bean urease.

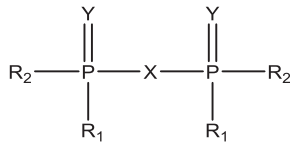

Comp	X	R_2	R_1	Y	pIC_{50}		$\Delta G_{binding}$ (kcal/mol)	IC_{50}(μM) ± SD[a]	Ref
					Exp	Pred			
01	ethane-1,2-diamino	phenyl	phenyl	O	1.56	1.31	−7.36	$2.7 \pm 0.21 \times 10^{-2}$	[23]
02	ethane-1,2-diamino	phenyl	phenyl	O	1.53	1.18	−7.45	$2.9 \pm 1.0 \times 10^{-2}$	[23]
03	butane-1,4-diamino	phenyl	phenyl	O	1.49	1.18	−7.26	$3.23 \pm 1.8 \times 10^{-2}$	[23]
04	piperazine-1,4-diyl	phenyl	phenyl	O	−0.28	0.15	−8.23	1.92 ± 0.05	[23]
05	2,2-dimethylpropane-1,3-diamino	phenyl	phenyl	O	1.55	1.30	−8.28	$2.8 \pm 1.6 \times 10^{-2}$	[23]
06	propane-1,2-diamino	phenyl	phenyl	O	1.53	1.35	−8.09	$2.9 \pm 1.2 \times 10^{-2}$	[23]
07	N,N'-dimethylethane-1,2-diamino	phenyl	phenyl	O	−0.36	−0.09	−8.1	2.32 ± 1.5	[23]
08	cyclohexane-1,2-diamino	phenyl	phenyl	O	2.45	2.40	−9.02	$3.5 \pm 1.87 \times 10^{-3}$	[23]
09	benzene-1,4-diamino	phenyl	phenyl	O	2.55	2.23	−8.42	$2.8 \pm 0.35 \times 10^{-3}$	–
10	4,4′-Biphenyldiamino	phenyl	phenyl	O	5.01	5.25	−8.53	$9.7 \pm 0.7 \times 10^{-6}$	[26]
11	(4,4′ methylene bis(phenyldiamino))	phenyl	phenyl	O	12.00	11.93	−9.24	$9.78 \pm 0.05 \times 10^{-13}$	–
12	(4,4′ ethylene bis(phenyldiamino))	phenyl	phenyl	O	12.71	12.63	−9.27	$1.91 \pm 0.03 \times 10^{-13}$	–
13	ethane-1,2 diamino	phenoxy	phenoxy	O	1.51	1.37	−7.02	$3.08 \pm 0.17 \times 10^{-2}$	[23]
14	propane-1,3 diamino	phenoxy	phenoxy	O	1.58	1.40	−7.58	$2.60 \pm 0.39 \times 10^{-2}$	[23]
15	butane-1,4-diamino	phenoxy	phenoxy	O	1.42	1.37	−6.3	$3.72 \pm 0.55 \times 10^{-2}$	[25]
16	piperazine-1,4-diyl	phenoxy	phenoxy	O	1.59	1.41	−7.71	$2.56 \pm 0.43 \times 10^{-2}$	[25]
17	benzene-1,4-diamino	phenoxy	Phenoxy	O	2.11	1.52	−8.26	$7.64 \pm 0.071 \times 10^{-3}$	[24]
18	4,4′-biphenyldiamino	phenoxy	phenoxy	O	2.46	1.93	−8.57	$3.41 \pm 0.03 \times 10^{-3}$	[26]
19	(4,4′ methylene bis(phenyldiamino))	phenoxy	phenoxy	O	2.53	2.56	−8.63	$2.90 \pm 0.55 \times 10^{-3}$	–
20	(4,4′ ethylene bis(phenyldiamino))	phenoxy	phenoxy	O	2.75	2.40	−7.64	$1.75 \pm 0.07 \times 10^{-3}$	–
21	ethane-1,2-diamino	phenoxy	phenyl amino	O	1.44	1.56	−6.68	$3.58 \pm 0.25 \times 10^{-2}$	[27]
22	propane-1,3-diamino	phenoxy	phenyl amino	O	1.52	1.65	−7.71	$3.02 \pm 0.05 \times 10^{-2}$	–
23	butane-1,4-diamino	phenoxy	phenyl amino	O	1.38	1.57	−6.71	$4.16 \pm 1.3 \times 10^{-2}$	[27]
24	piperazine-1,4-diyl	phenoxy	phenyl amino	O	1.62	1.47	−7.98	$2.37 \pm 0.10 \times 10^{-2}$	[25]
25	2,2-dimethylpropane-1,3-diamino	phenoxy	phenyl amino	O	1.45	1.43	−6.93	$3.48 \pm 0.3 \times 10^{-2}$	–
26	N,N'-dimethylethylenediamino	phenoxy	phenyl amino	O	1.65	1.26	−7.05	$2.20 \pm 0.29 \times 10^{-2}$	–
27	benzene-1,4-diamino	phenoxy	phenyl amino	O	1.59	1.92	−7.85	$2.56 \pm 1.6 \times 10^{-2}$	–
28	4,4′-Biphenyldiamino	phenoxy	phenyl amino	O	1.83	2.81	−8.36	$1.46 \pm 0.11 \times 10^{-2}$	–
29	ethane-1,2 diamino	ethoxy	ethoxy	S	−4.04	−4.04	−3.74	$1.12 \pm 0.06 \times 10^{+4}$	[22]
30	propane-1,3 diamin0	ethoxy	ethoxy	S	−4.08	−3.93	−3.45	$1.22 \pm 0.02 \times 10^{+4}$	[22]
31	butane-1,4-diamin0	ethoxy	ethoxy	S	−4.30	−4.05	−3.86	$2.00 \pm 0.03 \times 10^{+4}$	[22]
32	(piperazine-1,4-diyl)	ethoxy	ethoxy	S	−4.36	−4.11	−4.55	$2.30 \pm 0.01 \times 10^{+4}$	[22]
33	2,2-dimethylpropane-1,3-diamino	ethoxy	ethoxy	S	−4.25	−4.08	−4.06	$1.80 \pm 0.03 \times 10^{+4}$	[22]
34	benzene-1,4-diamino	ethoxy	ethoxy	S	−3.95	−4.09	−4.82	$9.00 \pm 0.09 \times 10^{+3}$	–
35	4,4′-Biphenyldiamino	ethoxy	ethoxy	S	−3.90	−4.11	−4.77	$8.00 \pm 0.29 \times 10^{+3}$	–
36	(4,4′ methylene bis(phenyldiamino))	ethoxy	ethoxy	S	−3.77	−4.09	−5.69	$6.00 \pm 0.03 \times 10^{+3}$	–
37	ethane-1,2 diamino	ethoxy	ethoxy	O	−0.35	−0.04	−3.46	2.28 ± 0.02	[22]
38	propane-1,3 diamin0	ethoxy	ethoxy	O	−0.06	−0.28	−3.67	1.17 ± 0.09	[22]
39	(piperazine-1,4-diyl)	ethoxy	ethoxy	O	0.04	−0.26	−4.54	$9.10 \pm 0.01 \times 10^{-1}$	[22]
40	benzene-1,4-diamino	ethoxy	ethoxy	O	0.55	0.86	−5.11	$2.80 \pm 0.07 \times 10^{-1}$	–
41	4,4′-biphenyldiamino	ethoxy	ethoxy	O	0.61	0.96	−5.08	$2.40 \pm 0.13 \times 10^{-1}$	–
42	(4,4′ methylene bis(phenyldiamino))	ethoxy	ethoxy	O	0.72	0.96	−5.99	$1.90 \pm 0.27 \times 10^{-1}$	–
43	(4,4′ ethylene bis(phenyldiamino))	ethoxy	ethoxy	O	1.44	1.56	−6.68	$1.70 \pm 0.22 \times 10^{-1}$	–

[a] Values are the mean ± SD.

of each hydrogen bond is 2.16 and 2.28 Å, respectively), the last interaction with length of 2.56 Å is found between the carbonyl oxygen of Asp 494 and the hydrogen of the amino group of **12**, (Fig. 5B). Moreover, two π–sulphur and π–alkyl interactions were found between two flap residues of the active site entrance (Cys592 and Arg439) and the phenyl rings of the amine chain, which resulted in a significant decrease in the enzyme activity in comparison with compounds containing aliphatic amines, as shown by Fig. 5A.

To further investigate the effect of π–interactions on the inhibitory potency of compounds due to the presence of phenyl rings in the structure of synthesized compounds, we performed a comparison (the k-mean clustering) between the aromatic index and the binding energy. The results showed that there is a reasonable relationship between them. As shown in Fig. 6, the compounds were classified into four categories. The compounds containing aromatic diamines are in the same category having less binding energy than other groups and thus have higher inhibitory power. According to the diagrams of the aromatic index relative to the free energy of binding, the structures containing the fewer number of phenyl rings have more binding energy. Information extracted from docking simulation reveals that compounds containing P=S substitutes have lower inhibitory activity than the P=O compounds, which is consistent with experimental results, (Fig. 6). In addition, further analysis of the results shows that the monophosphoramides have more binding energy than those of some bisphosphoramide derivatives, which can be attributed to the difference in their mode of interaction with the enzyme (Table S5). As mentioned above, bisphosphoramides are not able to interact with nickel ions due to their extended structure but cover the entire binding pocket. While monophosphoramides, thanks to their small structures, can easily enter the active site pocket of the urease enzyme and connect to the nickel

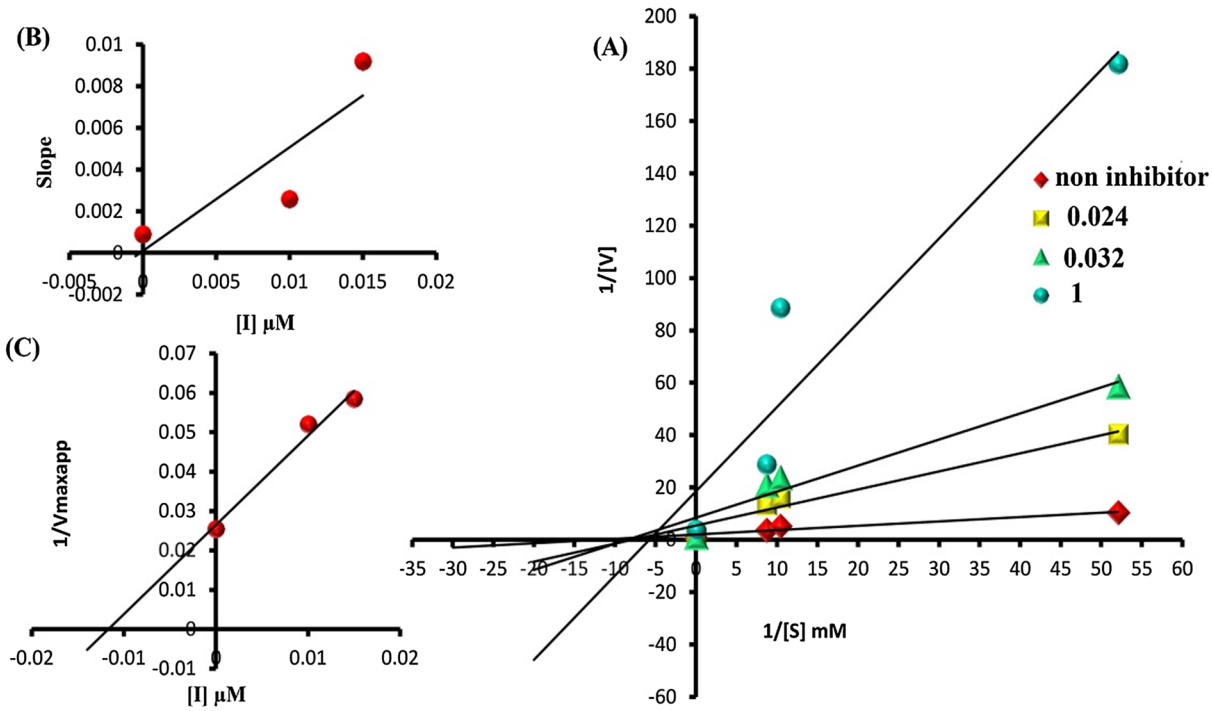

Fig. 4. (A) Lineweaver-Burk plot of the inhibition of the jack bean urease activity in the absence and in presence of compound 12. (B) and (C) secondary replots of the Lineweaver–Burk plot, slope and $1/V_{max}$ app versus various concentrations of compound 12, respectively.

ions inside of its active site [1,5,6,15]. Following these studies, the QSAR study was conducted to achieve a logical relationship between the activity and structure of the compounds.

2.6. QSAR analysis

QSAR calculations were performed to determine the most important descriptors affecting the inhibitory power using Genetic Algorithm and Artificial Neural Network (GA–ANN) method. Of the 101 structural and electronic descriptors, six descriptors were selected as the most important descriptors using the GA method, which are: rotatable bond fraction (*RBF*), ^{31}P chemical shift (δ), total energy of the molecule (E_{total}), total charge (Q_{total}), the number of aromatic and aliphatic rings (*nCIC*), and the number of aromatic bonds (*nAB*). These six selected

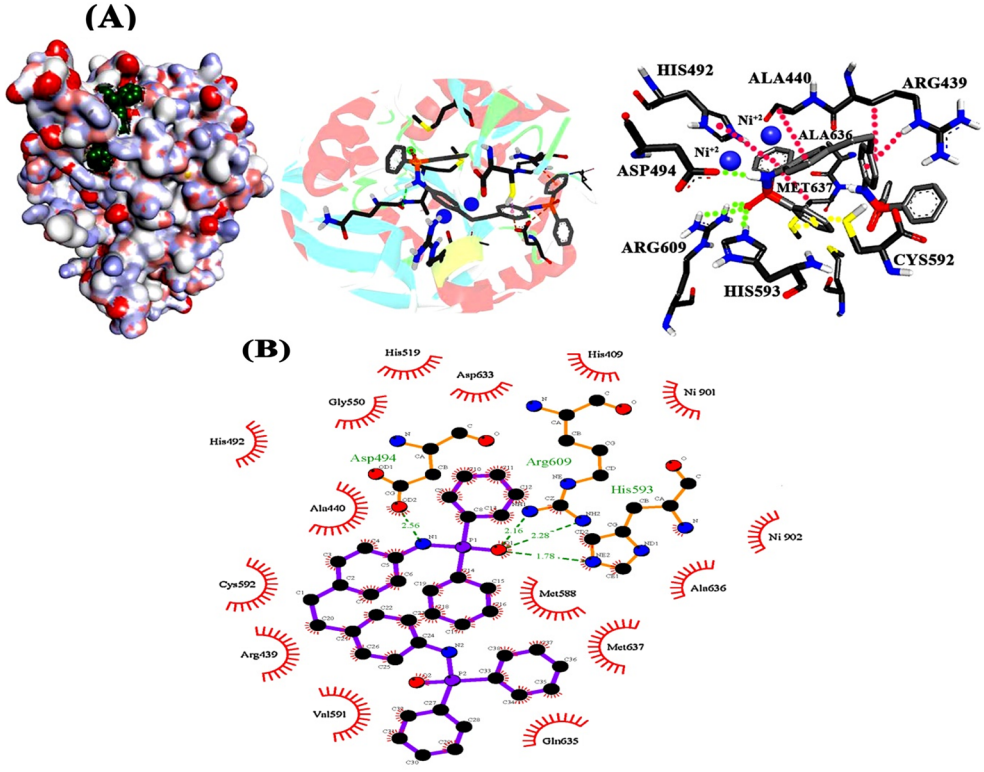

Fig. 5. Plausible binding mode of the most active compound **(12)** within the binding pocket of jack bean urease: (A) left: The enzyme and inhibitor are shown as surface and cpk in green color, respectively, which indicates the entire coverage of the binding pocket by the inhibitor; (A) middle: The enzyme and **12** are demonstrated as ribbon and stick forms, respectively; (A) right: The dotted lines illustrate various interactions between **12** and the active site residues, which including hydrogen bond (green), π–sulphur (yellow) and π–alkyl (pink) interactions. For clarity only interacting residues are labeled; the two nickel ions are represented as blue spheres. (B) 2D interaction diagram of **12** with the target enzyme. Hydrogen bond interactions are indicated with green dashed lines.

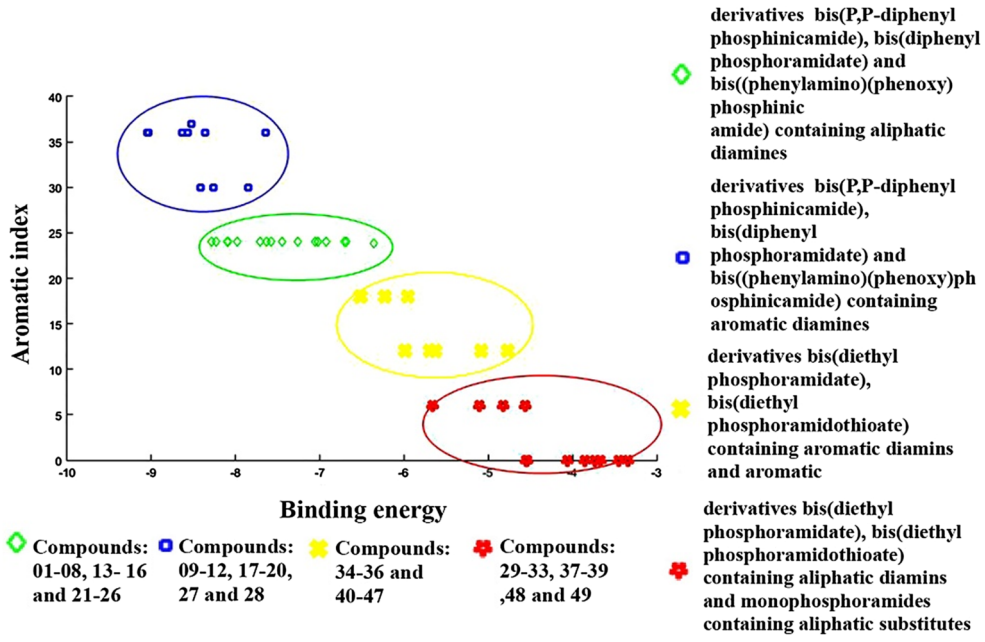

Fig. 6. Clustering of compounds (assayed bis and mono phosphoramides) based on binding energy and aromatic index.

Table 4
Statistical parameters obtained from the QSAR model.

GA-ANN	Validation				Training	
	Q^2_{LOO}	$RMSE_{LOO}$	R^2_{L6O}	$RMSE_{L6O}$	R_t^2	$RMSE_t$
	0.827	1.355	0.804	1.805	0.988	0.331

R_t^2 is a correlation coefficient of the training set; $RMSE_t$ is a root mean square error of the training set.
Q^2_{LOO} is a correlation coefficient of leave-one-out cross validation, $RMSE_{LOO}$ is a root mean square error LOO–CV.

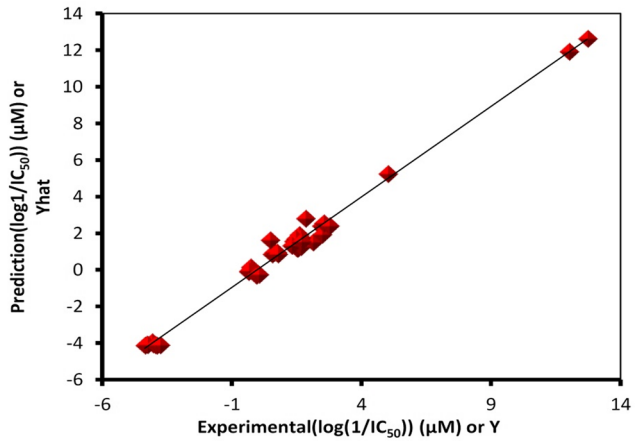

Fig. 7. Plot of experimental pIC_{50} versus predicted pIC_{50} of assayed bis and mono phosphoramides by GA–ANN model.

descriptors and –logIC_{50} were used as input and output of the ANN model, respectively. The statistical parameters obtained from the model such as correlation coefficient (R^2) and root mean square error (*RMSE*) are 0.988 and 0.331, respectively, which indicates a strong correlation between independent and dependent variables and appropriate accuracy of the model shown in Table 4. The predicted –logIC_{50} values are presented in Table 3, and the relationship between experimental and predicted values of biological activity is illustrated in Fig. 7.

To further study the validity of the model used, Leave-One-Out (*LOO*) and Leave-Multiple-Out (*LMO*) cross-validation methods were used. In the first cross-validation model, a molecule is considered as a prediction set and the model is developed using other molecules. However, in the second cross-validation model, the numbers of molecules (M) are set aside as a prediction set. In the LMO method, we set the M equal to six, and the L6O model was repeated 200 times. The data from LOO and L6O cross-validations are shown in Table 4. The high values of Q^2_{LOO} and R^2_{L6O} are indicative of the stability and the predictive ability of the generated model.

According to the diagram of the selected descriptors importance (shown in Fig. 8), molecule total energy descriptor (E_{total}) has the most significance among chosen descriptors. The study of the total energy of the synthesized compounds indicated that the bisphosphoramide compounds have lower total energy and are more stable than the monophosphoramide compounds synthesized in this work. Another important factor affecting inhibitory activity is the *nCIC* descriptor which represents the number of rings in the structure of the compounds and is associated with the number of aromatic and aliphatic rings, whose presence in the construction of molecules provides information on the hydrophobicity and rigidity of the compounds.

Investigating the effect of the number of rings on inhibitory activity showed that increasing the number of rings in the structure has a positive impact on the value of pIC_{50}, which can be due to an increase in the number of hydrophobic and π interactions between the enzyme and the inhibitor as can be seen in Fig. 9. The *RBF* descriptor represents the

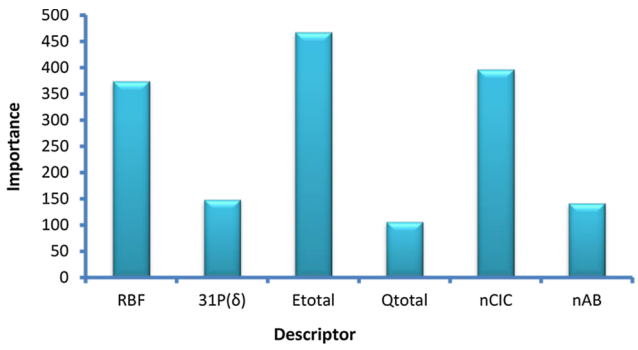

Fig. 8. Relative importance of the selected descriptors in GA-ANN model.

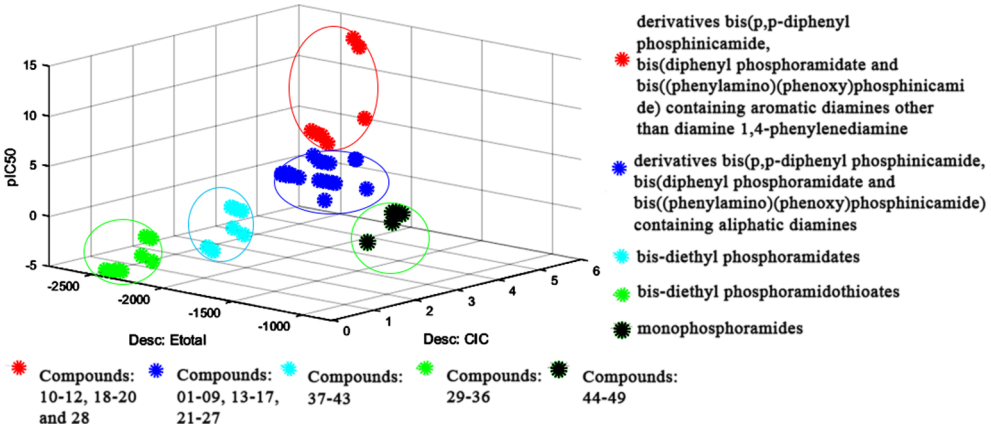

Fig. 9. Relationship and changes of pIC_{50} values of assayed all compounds relative to E_{total} and *nCIC*.

flexibility and rigidity of compounds and is influenced by the type of bond and the number of carbon atoms and the nature of substituents (such as aromatic and aliphatic substituents) in the compounds. The phosphorus chemical shift is the third most important descriptor that is altered by changing the functional groups attached to the phosphorus atom. The study of the relationship between pIC_{50} and chemical shift of phosphorus showed that the oxygen and sulfur atoms connected to the phosphorus atoms have the largest effect on the chemical shift of phosphorus atoms. Thus, in terms of the chemical shift of phosphorus, the compounds were classified into two groups: P═O with chemical shift in the range of –7.3 to 31.56 ppm and P═S with chemical shift in the range of 63.73–76.59 ppm. It has also been observed in the inhibitory behavior of these compounds that the ones with P═S moiety had less inhibitory activity than those with a P═O moiety, as shown in Fig. 9. The total charge descriptor (Q_{total}) is influenced by heteroatoms and hydrogen bond donor and acceptor groups in the structure of compounds that significantly affect the inhibitory potency.

2.7. Analysis of molecular electrostatic potential (MESP)

In order to rationalize the results of theoretical and empirical studies on the inhibition of most of the derivatives containing the P═O functional group in comparison to the compounds containing the P═S functional group and determining the reactive sites in the structure of the molecules, their molecular electrostatic potential (MESP) surfaces were calculated using the B3LYP/6–311 + G** method. The color spaces in the MESP maps represent the electrostatic potential. The red area is an electron-rich region and a nucleophilic center in the structure, the blue part is an electron deficient region known as the electrophilic center, and the yellow areas are less electron rich regions. As shown in Fig. 10, from the comparison of electrostatic potential maps of compounds **11** and **36**, it can be concluded that the oxygen atoms attached to the phosphorus atoms, were located in the red areas and have the most negative potential than sulfur atoms, which represents their strong tendency to participate in nucleophilic reactions. Blue regions that describe electropositive regions or electron deficiency regions are located on the hydrogen atoms attached to nitrogen atoms and contribute as electron receptors to the interactions between the inhibitor and the enzyme. The yellow color of the phenyl rings is due to the delocalized electrons of the phenyl rings, which have an influence on the formation of π-interactions and increasing the inhibitory activity of the compounds.

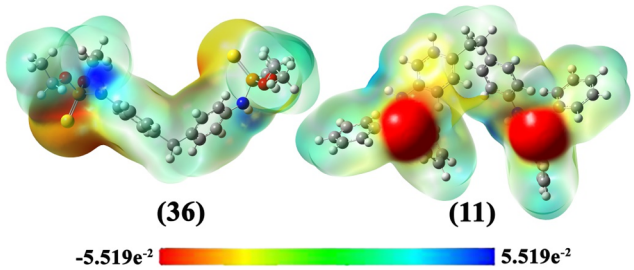

Fig. 10. Comparison of the electrostatic potential surfaces of compounds 11 and 36. In this diagram, the red and blue areas indicate the richest density electron region and the poorest one.

3. Conclusions

Investigating the results of the bisphosphoramide derivatives inhibitory test showed that these derivatives have a different behavior as compared to monophosphoramide compounds regarding the type of inhibitory mechanism (they have a mixed type inhibitory mechanism) and the ability to inhibit urease enzymes (with the inhibitory range of 23,000–1.91 × 10^{-13} μM). The docking analysis revealed that these compounds are connected to the key residues of the entrance and inside of the binding pocket via hydrogen bonds, hydrophobic and π–interactions. It has also been found that these compounds do not interact directly with nickel because of their extended structures, but react with other active site residues and occupy the entire binding pocket, which was supported by information derived from kinetic studies. The results obtained from docking analysis and experimental studies similarly indicated that the derivatives containing aromatic amines in their structure have more inhibitory activity than derivatives containing aliphatic amines. Also, in a closer examination, it was determined that inhibitors containing the P═O functional group are more potent than the inhibitors containing P═S. Following these studies, QSAR calculations were performed to determine the most significant descriptors affecting the inhibitory activity of the synthesized bisphosphoramides using the Genetic Algorithm and the Artificial Neural Network (GA–ANN) method. The total energy of the molecule (E_{total}), the number of rings (*nCIC),* a rotatable bond fraction (*RBF*), ^{31}P chemical shift (δ), the number of aromatic bonds (*nAB*) and total charge (Q_{total}) descriptors were selected as the most critical parameters influencing the inhibitory activity. The chemical shift of phosphorus atoms is one of the parameters affecting the inhibitory power of these compounds. The sulfur and oxygen atoms connected to the phosphorus atom are the main factors in chemical shift and differences in the ability of the inhibitors. These differences were justified by analysis of molecular electrostatic potential surfaces of the compounds. In general, the logical relations between theoretical and empirical results shows that an increase in effective functional groups (P═O, P—N, and aromatic substitutes) in the compounds, despite extending the structure, has a

positive effect on the inhibitory activity by changing the type of mechanism and the interaction model of the inhibitor with the enzyme. This information can be used as an introduction to the synthesis of targeted inhibitors.

4. Materials and methods

4.1. Instruments

All chemicals and solvent were purchased from commercial suppliers (Sigma–Aldrich, Merck) and all of them were of reagent grade and were used without further purification. Nuclear magnetic resonance spectra (NMR) were recorded on a Bruker Avance DRX 500 MHz spectrometer. TMS (tetramethylsilane) in ^{1}H and ^{13}C NMR spectroscopy and H_3PO_4 85% in ^{31}P NMR spectroscopy were used as internal standards. Infrared spectra (IR) were recorded on a Nicolet 510P spectrophotometer using KBr disks. Melting points were determined by an electrothermal instrument. UV–Vis spectra were recorded on a Perkin–Elmer Lambda 25 spectrophotometer. Instrumentation details for the single crystals X-ray analysis of **22** and **26** are provided in the supporting information. Crystallographic data of **22** and **26** have been deposited with the CCDC and have been given the deposition numbers 1,581,447 and 1,584,194 for **22** and **26**, respectively. Molecular docking simulations were performed to obtain the ligand-protein interaction information using the ADT software (AutoDockTools package, version 1.5.6) along with AutoDock 4.2 and hybrid Lamarckian Genetic Algorithm (LGA) [33]. The three-dimensional crystal structure of jack bean urease was obtained with 1.49 Å resolutions from the Protein Data Bank (PDB code: 4GY7).

4.2. Synthesis

Compounds (**01–08**), **10**, (**13–18**), **21**, **23**, **24**, (**29–33**) and (**37–39**) were synthesized and characterized according to the procedure reported in our previous work [22–27]. The synthesis procedures and information relating to the identification of compounds **09**, (**11–12**), (**19**, **20**, **22**), (**25–28**), (**34–36**) and (**40–43**) are provided in the Supporting Information. Fig. 1 shows the newly synthesized compounds in this work.

4.3. Urease inhibition assay

Urease inhibitory activity was determined by measuring the absorption of ammonia released using the indophenol method which has been explained by Weather Burn [34]. At first, 1 mL of buffer solution (NaH_2PO_4/Na_2HPO_4, 70 mM, pH 7.4), 1 mL of inhibitor solution with different concentrations (in order to dissolve some of the compounds, a mixture of water and dimethyl sulfoxide solvents was used; the highest concentration of dimethyl sulfoxide used in the assays was 4%.), and 10 μL of jack bean urease solution (2.5 mg/mL, 12.5 U/mL) were mixed together in test tubes and incubated for 30 min at 37 °C. Then, 1 mL of urea solution (6 mg/mL) was added to the assay mixture and again was incubated for 30 min at 37 °C. Afterward, 1 mL of phenol reagent (1.0 g phenol, 5 mg sodium nitroprusside in 100 mL water) was added to the mixture. After mixing, 1 mL of alkali reagent (0.5 g NaOH, 870 μL sodium hypochlorite in 100 mL water) was added and the final mixture was incubated for 30 min at 37 °C. The absorbance of the resulting colored mixture was measured using UV–Vis spectrophotometer at 625 nm. The control solution contained the same mix without inhibitor. The inhibitory assays for all compounds were performed in triplicate, and phenylphosphorodiamidate (PPD) was used as reference inhibitor in the inhibitory assay. The inhibition percentage [INH (%)] was calculated using the following formula:

$$\mathrm{INH}(\%) = 100 - ((A_{\mathrm{INH}}/A_B) \times 100) \quad (1)$$

where A_B and A_{INH} are the absorbances of control solution and inhibitor solution, respectively. The IC_{50} values for urease inhibition were determined using the non-linear curve fitting program PRISM 6.07 (GraphPad Prism).

4.4. Kinetics study

Lineweaver-Burk plots of the velocities inverse value ($1/v$) versus the substrate concentration inverse value ($1/[Urea]$) were applied to determine the mechanism of enzyme inhibitory in synthesized bisphosphoramide compounds. The values of kinetic parameters (K_m, V_{max}) were determined using these plots in the absence and presence of inhibitor and at different concentrations of urea. V_{max}^{app}. and K_m^{app} values were determined for at least 4 concentrations of inhibitor. The values of K_i and K_I inhibitory constants were determined using two plots. The first of which is plot of $1/V_{max}$ vs. different concentrations of inhibitor, and other plot is the plot of the slope vs. inhibitor concentration. The intersection of each of them on the x-axis will be equivalent to $-K_I$ and $-K_i$, respectively. In this study, the slopes were obtained from the Lineweaver–Burk lines.

4.5. QSAR calculations

To obtain a quantitative relationship between structure and biological activity, the QSAR model was used. In this model, pIC_{50} is considered as the dependent variable and molecular structure descriptors as independent variables. The molecular descriptors were calculated using the following methods.

Before computing molecular descriptors, all of the 49 compounds were fully optimized at the B3LYP/6–311 + G** level [35] using the Gaussian 09 program package [36] in the solvent phase (solvent: water). In the present work, part of the molecular descriptors were calculated using Dragon 3.0 software [37], including: constitutional descriptors, 2D-atom pairs, 3D-atom pairs, charge descriptors, functional group counts, atom-centered fragment. Another part of the electronic and structural descriptors was generated by the quantum chemical calculations and theoretical studies [38]. Descriptors obtained by this method are as follows: The energy of the lowest unoccupied molecular orbital (E_{LUMO}), the energy of the highest occupied molecular orbital (E_{HOMO}), the energy difference between the HOMO and LUMO (ΔE_{L-H}), polarizability (PL, the charge difference between the atoms in functional groups) [39], the net atomic charges (Q), and ^{31}P and ^{1}H NMR chemical shifts (δ) [40], dipole moment (μ) and molecular volume (Mv), bond lengths and bond angles around the phosphorus atoms, electrophilicity (ω) [41] and hydrophobic coefficient (log P). All of the electronic descriptors were extracted from the DFT results [42,43] by using the Gaussian 09 program package. In general, by removing descriptors that have the same values for all molecules as well as removing one of two pairs of descriptors that have a correlation coefficient greater than 0.90, in total, only 101 descriptors were used in QSAR studies. The calculated values of some descriptors for each compound are listed in Table S4. Since nonlinear methods consider both linear and nonlinear properties between dependent and independent variables, nonlinear means are more suitable for selecting descriptors. Due to the nonlinear relationship between dependent and independent variables in the present work, the technique of Genetic Algorithm- Artificial Neural Networks (GA–ANN) was used to select the best molecular descriptors related to biological activity [44], which were performed using MATLAB software (version 8.5.0 (R2015a)). In the technique GA–ANN, GA is a random optimization method based on evolutionary optimization and ANN is used as a fitness function in GA

[44]. Selected descriptors were used as inputs of the ANN model to build the QSAR model (GA–ANN). A population of 50 chromosomes and two nodes in a hidden layer are part of the parameters that were used to generate this model. Finally, to evaluate the performance of the developed QSAR model, the parameters of the root mean square error (*RMSE*) and coefficient of determination (R^2) were used. Leave–One–Out (LOO–CV) and Leave–Multiple–Out (LMO–CV) cross-validation techniques were applied to authenticate the generated model.

4.6. Protocol of docking study

AutoDock 4.2 software was employed for docking analysis. The crystal structure of Jack bean urease (PDB ID: 4GY7) was selected for these studies. The stable geometry structures of the compounds were fully optimized using the Density Functional Theory (DFT) at the B3LYP/6–311 + G** level of theory [35]. More details about the docking steps are provided in the Supporting Information. The binding free energy was calculated using the AutoDock 4.2 program according to Eq. (2). The LIGPLOT program (version v.1.4.5) was used to show the 2D ligand-enzyme interactions [45]. The view of the docking results and analysis of their surface with graphical representations were done using AutoDockTools and discovery studio visualizer [46].

$$\Delta G_{\text{binding}} = [\Delta G_{\text{intermolecular}} + \Delta G_{\text{internal}} + \Delta G_{\text{torsional}}] - [\Delta G_{\text{unbound}}] \quad (2)$$

Acknowledgements

Financial support of this work by Tarbiat Modares University is gratefully acknowledged.

Conflict of interest

The authors declare no conflict of interest.

Appendix A. Supplementary material

Supplementary data to this article can be found online at https://doi.org/10.1016/j.bioorg.2019.01.064.

References

[1] M. Font, M.a.J. Domínguez, C. Sanmartín, J.A. Palop, S. San-Francisco, O. Urrutia, F. Houdusse, J.M. García-Mina, Structural characteristics of phosphoramide derivatives as urease inhibitors. Requirements for activity, J. Agr. Food Chem. 56 (2008) 8451–8460.
[2] B. Krajewska, I. Ureases, Functional, catalytic and kinetic properties: a review, J. Mol. Catal. B:enzym. 59 (2009) 9–21.
[3] K. Sahrawat, Control of urea hydrolysis and nitrification in soil by chemicals—Prospects and problems, Plant. Soil. 57 (1980) 335–352.
[4] K. Macegoniuk, E. Grela, J. Palus, E. Rudzińska-Szostak, A. Grabowiecka, M. Biernat, Ł. Berlicki, 1, 2-Benzisoselenazol-3 (2 H)-one derivatives as a new class of bacterial urease inhibitors, J. Med. Chem. 59 (2016) 8125–8133.
[5] L. Mazzei, M. Cianci, U. Contaldo, F. Musiani, S. Ciurli, Urease inhibition in the presence of N-(n-Butyl) thiophosphoric triamide, a suicide substrate: structure and kinetics, Biochemistry. 56 (2017) 5391–5404.
[6] M.a.J. Domínguez, C. Sanmartín, M.a. Font, J.A. Palop, S. San Francisco, O. Urrutia, F. Houdusse, J.M. García-Mina, Design, synthesis, and biological evaluation of phosphoramide derivatives as urease inhibitors, J. Agr. Food Chem. 56 (2008) 3721–3731.
[7] K.A. Eaton, C. Brooks, D. Morgan, S. Krakowka, Essential role of urease in pathogenesis of gastritis induced by Helicobacter pylori in gnotobiotic piglets, Infect. Immun. 59 (1991) 2470–2475.
[8] S. Kiss, M. Simihaian, Improving Efficiency of Urea Fertilizers by Inhibition of Soil Urease Activity, Springer Science & Business Media, 2013.
[9] K. Macegoniuk, A. Dziełak, A. Mucha, Ł. Berlicki, Bis (aminomethyl) phosphinic acid, a highly promising scaffold for the development of bacterial urease inhibitors, ACS Med. Chem. Lett. 6 (2014) 146–150.
[10] L. Macomber, M.S. Minkara, R.P. Hausinger, K.M. Merz Jr, Reduction of urease activity by interaction with the flap covering the active site, J. Chem. Inf. Model. 55 (2015) 354–361.
[11] H. Mobley, R. Hausinger, Microbial ureases: significance, regulation, and molecular characterization, Microbiol Rev. 53 (1989) 85–108.
[12] J.C. Rutherford, The emerging role of urease as a general microbial virulence factor, PLoS Pathog. 10 (2014) e1004062.
[13] J. Bremner, H. Chai, Effects of phosphoroamides on ammonia volatilization and nitrite accumulation in soils treated with urea, Biol. Fert. Soils. 8 (1989) 227–230.
[14] N.E. Dixon, C. Gazzola, J.J. Watters, R.L. Blakeley, B. Zerner, Inhibition of jack bean urease (EC 3.5. 1.5) by acetohydroxamic acid and by phosphoramidate. Equivalent weight for urease, J. Am. Chem. Soc. 97 (1975) 4130–4131.
[15] W.S. Faraci, B.V. Yang, D. O'Rourke, R.W. Spencer, Inhibition of Helicobacter pylori urease by phenyl phosphorodiamidates: mechanism of action, Bioorgan. Med. Chem. 3 (1995) 605–610.
[16] F. Kolc, D. Swerdloff, US Patent 4,530,714, 1985, in: Chem. Abstr. 1985, pp. 61450t.
[17] A.J. Pope, N. Toseland, B. Rushant, S. Richardson, M. Mcvey, J. Hills, Effect of potent urease inhibitor, fluorofamide, on Helicobacter sp. in vivo and in vitro, Digest. Dis. Sci. 43 (1998) 109–119.
[18] A. Mucha, P. Kafarski, Ł. Berlicki, Remarkable potential of the α-aminophosphonate/phosphinate structural motif in medicinal chemistry, J. Med. Chem. 54 (2011) 5955–5980.
[19] S. Vassiliou, A. Grabowiecka, P. Kosikowska, A. Yiotakis, P. Kafarski, Ł. Berlicki, Design, synthesis, and evaluation of novel organophosphorus inhibitors of bacterial ureases, J. Med. Chem. 51 (2008) 5736–5744.
[20] B. Krajewska, W. Zaborska, Jack bean urease: The effect of active-site binding inhibitors on the reactivity of enzyme thiol groups, Bioorg. Chem. 35 (2007) 355–365.
[21] G. McCarty, J. Bremner, J. Lee, Inhibition of plant and microbial ureases by phosphoroamides, Plant. Soil. 127 (1990) 269–283.
[22] K. Gholivand, A.A. Ebrahimi Valmoozi, M. Bonsaii, Synthesis and crystal structure of new temephos analogues as cholinesterase inhibitor: molecular docking, QSAR study, and hydrogen bonding analysis of solid state, J. Agr. Food Chem. 62 (2014) 5761–5771.
[23] K. Gholivand, A.A. Ebrahimi Valmoozi, M. Rahimzadeh Dashtaki, F. Mohamadpanah, M. Dusek, V. Eigner, M. Pooyan, M. Bonsaii, M. Sharifi, M. Ghadamyari, Synthesis, Crystal structure, fluorescence assay, molecular docking and QSAR/QSPR studies of temephos derivatives as human and insect cholinesterase inhibitors, ChemistrySelect 2 (2017) 8828–8840.
[24] K. Gholivand, A. Gholami, A. Ebrahimi, S. Abolghasemi, M. Esrafili, F. Fadaei, K. Schenk, Triphenyltin (IV) adducts of diphosphoryl ligands: structural, electronic and energy aspects from X-ray crystallography and theoretical calculations, RSC Adv. 5 (2015) 17482–17492.
[25] K. Gholivand, M. Hosseini, A.A.E. Valmoozi, K. Farshadfar, Polymorphism, pseudopolymorphism, and conformerism in the crystal structure of piperazine-N, N′-bis (N, O-diphenyl phosphoramidate), CrystEngComm. 19 (2017) 2536–2548.
[26] K. Gholivand, A.A.E. Valmoozi, M. Salahi, F. Taghipour, E. Torabi, S. Ghadimi, M. Sharifi, M. Ghadamyari, Bisphosphoramidate derivatives: synthesis, crystal structure, anti-cholinesterase activity, insecticide potency and QSAR analysis, J. Iran. Chem. Soc. 14 (2017) 427–442.
[27] M.B. Gholivand, L. Mohammadi-Behzad, G. Paimard, K. Gholivand, A.A.E. Valmoozi, Electrochemical characterization of some bisphosphoramidates spiked carbon paste electrodes and their applications in DNA sensing, J. Electroanal. Chem. 742 (2015) 62–69.
[28] L. Asadi, K. Gholivand, K. Zare, Phosphorhydrazides as urease and acetylcholinesterase inhibitors: biological evaluation and QSAR study, J. Iran. Chem. Soc. 13 (2016) 1213–1223.
[29] K. Gholivand, A. Gholami, S. Tizhoush, K. Schenk, F. Fadaei, A. Bahrami, Steric and electronic control over the structural diversity of N-(n-pyridinyl) diphenylphosphinic amides (n = 2 and 4) as difunctional ligands in triphenyltin (IV) adducts, RSC Adv. 4 (2014) 44509–44516.
[30] B. Bano, K.M. Khan, A. Lodhi, U. Salar, F. Begum, M. Ali, M. Taha, S. Perveen, Synthesis, in vitro urease inhibitory activity, and molecular docking studies of thiourea and urea derivatives, Bioorg. Chem. (2018).
[31] M.K. Rauf, A. Talib, A. Badshah, S. Zaib, K. Shoaib, M. Shahid, U. Floerke, J. Iqbal, Solution-phase microwave assisted parallel synthesis of N, N′-disubstituted thioureas derived from benzoic acid: biological evaluation and molecular docking studies, Eur. J. Med. Chem. 70 (2013) 487–496.
[32] K.-F. Chan, I.L. Wong, J.W. Kan, C.S. Yan, L.M. Chow, T.H. Chan, Amine linked flavonoid dimers as modulators for P-glycoprotein-based multidrug resistance: structure–activity relationship and mechanism of modulation, J. Med. Chem. 55 (2012) 1999–2014.
[33] G.M. Morris, D.S. Goodsell, R.S. Halliday, R. Huey, W.E. Hart, R.K. Belew, A.J. Olson, Automated docking using a Lamarckian genetic algorithm and an empirical binding free energy function, J. Comput Chem. 19 (1998) 1639–1662.
[34] M. Weatherburn, Phenol-hypochlorite reaction for determination of ammonia, Anal. Chem. 39 (1967) 971–974.
[35] A.E. Reed, L.A. Curtiss, F. Weinhold, Intermolecular interactions from a natural bond orbital, donor-acceptor viewpoint, Chem. Rev. 88 (1988) 899–926.
[36] M. Frisch, G. Trucks, H. Schlegel, G. Scuseria, M. Robb, J. Cheeseman, G. Scalmani, V. Barone, B. Mennucci, G. Petersson, Gaussian 09, revision b. 01, Gaussian, Inc., Wallingford, CT. 6492, 2010.
[37] R. Todeschini, V. Consonni, A. Mauri, M. Pavan, Software Dragon: Calculation of Molecular Descriptors, Department of Environmental Sciences, University of Milano-Bicocca and Talete, srl, Milan, Italy, 2003.
[38] E.B. de Melo, Multivariate SAR/QSAR of 3-aryl-4-hydroxyquinolin-2 (1H)-one derivatives as type I fatty acid synthase (FAS) inhibitors, Eur. J. Med. Chem. 45 (2010) 5817–5826.
[39] R. Hu, J.-P. Doucet, M. Delamar, R. Zhang, QSAR models for 2-amino-6-

arylsulfonylbenzonitriles and congeners HIV-1 reverse transcriptase inhibitors based on linear and nonlinear regression methods, Eur. J. Med. Chem. 44 (2009) 2158–2171.
[40] S. Ghadimi, A.A. Ebrahimi Valmoozi, M. Pourayoubi, K. Asad, Samani, Structure-activity study of phosphoramido acid esters as acetylcholinesterasf inhibitors, J. Enzym Inhib Med Ch. 23 (2008) 556–561.
[41] R.G. Parr, L.v. Szentpaly, S. Liu, Electrophilicity index, J. Am. Chem. Soc. 121 (1999) 1922–1924.
[42] J. Foster, F. Weinhold, Natural hybrid orbitals, J. Am. Chem. Soc. 102 (1980) 7211–7218.
[43] K. Gholivand, A.A. Ebrahimi Valmoozi, H.R. Mahzouni, S. Ghadimi, R. Rahimi, Molecular docking and QSAR studies: noncovalent interaction between acephate analogous and the receptor site of human acetylcholinesterase, J. Agr. Food Chem. 61 (2013) 6776–6785.
[44] L. Wang, A hybrid genetic algorithm–neural network strategy for simulation optimization, Appl. Math. Comput. 170 (2005) 1329–1343.
[45] A.C. Wallace, R.A. Laskowski, J.M. Thornton, LIGPLOT: a program to generate schematic diagrams of protein-ligand interactions, Protein Eng. 8 (1995) 127–134.
[46] D. Systemes, BIOVIA, Discovery Studio Modeling Environment. Release 4.5, Dassault Systemes, San Diego, CA, 2015.